Jour. Petrol. Soc. Korea
Vol. 3, No. 1, p. 94~108, 1994

Metamorphism of the Hongjesa granite and the adjacent metasedimentary rocks

(Magmatism and metamorphism of the Proterozoic in the northeastern part of Korea)

Jeongmin Kim, Moonsup Cho and Hyung Shik Kim*

Department of Geological Sciences, Seoul National University, Seoul, 151-742 Korea
**Department of Geology, Korea University, Seoul, 135-701 Korea*

ABSTRACT : The Precambrian Hongjesa granite, and the Yuli group and the Hyeondong gneiss complex are studied to unravel the metamorphic history of the northeastern Sobaeksan massif. The Hongjesa granite, emplaced at 650-700℃ and 3±1 kbar, has been altered at 310-568℃. Not only the chloritization of biotite but also the sericitization and saussuritization of plagioclase occur at the subsolidus stage. Biotites of the Hongjesa granite vary in their Al, Fe and Mg contents through dioctahedral and tschermakitic substitutions during the subsolidus stage. Secondary muscovites from biotite and feldspars are enriched in their Si and Mg+Fe contents through tschermakitic and trioctahedral substitutions. The metamorphic pressures and temperatures estimated from the Hyeondong gneiss complex are 3.6-6.6 kbar and 593-718℃, respectively. Local migmatization producing the cordierite-bearing assemblage occurs in the Hyeondong gneiss complex. The Gibbs' method applied to the assemblage of garnet+biotite+plagioclase+quartz in banded gneiss suggests a complex P-T history of the Hyeondong gneiss complex.

Key Words : Hongjesa granite, Hyeondong gneiss complex, Gibbs' method, migmatization

INTRODUCTION

The northeastern Sobaeksan massif of this study consists of Precambrian granitoids together with the metamorphic rocks of the Yuli group and the Hyeondong gneiss complex (Fig. 1). The overall tectono-metamorphic and -magmatic relations of this massif are not revealed yet, although several geochemical and petrologic studies are available (Lee and Kim, 1984; Kim *et al.*, 1986; and Kim *et al.*, 1991). Kim *et al.* (1986) have estimated the metamorphic condition of the study area to be 600-700℃ and 4-6 kbar, based on mineral parageneses of xenoliths in the Hongjesa granite and metasedimentary rocks of the Yuli group. However, the detailed reaction mechanism of the subsolidus recrystallization and the P-T condition of the Hongjesa granite have been little investigated by previous workers.

In the accompanying paper (Kim and Cho, 1994), we have discussed the petrogenesis of the Hongjesa granite. In this paper, we focus on determining the physicochemical conditions responsible for the subsolidus alteration of the Hongjesa granite and the metamorphism of its adjacent metasedimentary rocks, primarily based on mineral chemistry and phase equilibria. The purposes of this study are: (1) to characterize the subsolidus recrystallization of the Hongjesa granite; (2) to estimate the P-T condition of the Hongjesa granite during and after the emplacement; and finally (3) to determine the metamorphic conditions of the Yuli group and the Hyeondong gneiss complex and to compare the result with that of the Hongjesa granite.

GENERAL GEOLOGY

Lee and Kim (1984) have divided the metasedimentary rocks of the Taebaeksan region

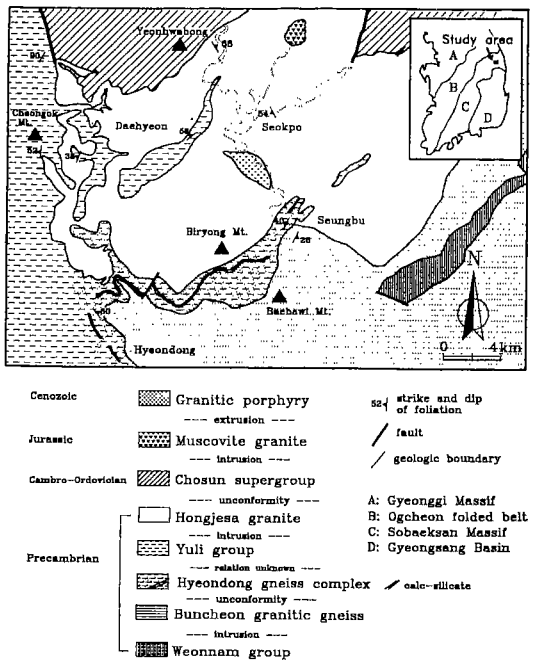

Fig. 1. Location and geologic map of the study area (modified after Kim and Lee, 1983).

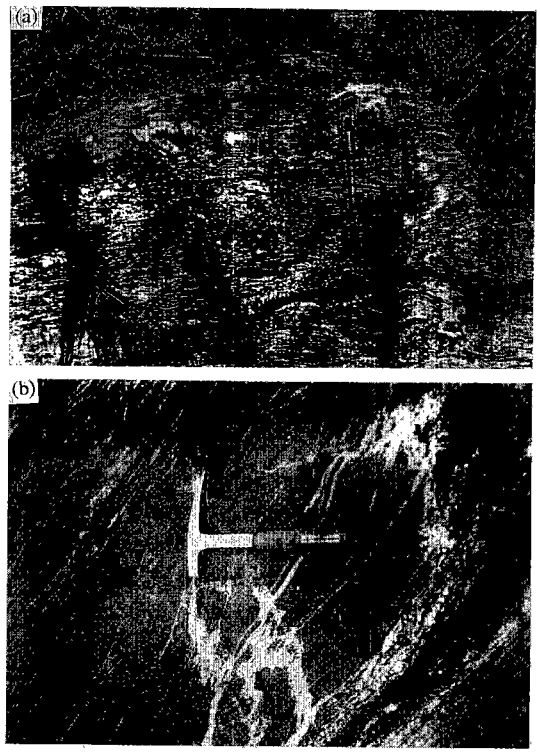

Fig. 2. Outcrop photographs of migmatitic gneiss in the Hyeondong gneiss complex. (a) Leucosomes alternating with melanosomes. (b) Leucosomes cross-cutting the amphibolitic layer.

into the Taebaeksan schist complex and the Taebaeksan gneiss complex on the basis of mineral paragenesis and metamorphic grade. Kim *et al.* (1986) have designated the high-grade metasedimentary rocks containing calc-silicate layer near the Hyeondong-Seungbu area as the Hyeondong schist complex (Fig. 1). Because this complex mainly consists of high-grade gneiss and amphibolite, we use the term Hyeondong gneiss complex, as suggested by Kim (1991). The metasedimentary rocks in the western part of the Hongjesa granite are referred to as the Yuli group in this study. The boundary between these rock units (Fig. 1) is only an approximation, although amphibolitic and calc-silicate layers occur only in the Hyeondong gneiss complex.

The contact relations between granite and country rock together with the occurrence of xenoliths similar to the country rocks suggest that the Hongjesa granite has intruded the Yuli group and the Hyeondong gneiss complex. The latter metamorphic units commonly show at least two different sets of metamorphic fabrics, whereas the Hongjesa granite is free of any penetrative deformation.

The Hyeondong gneiss complex consists primarily of banded gneiss, amphibolite, hornblende-biotite schist, migmatitic gneiss, calc-silicate rock and quartzite. In particular, the calc-silicate layer forms a mappable unit throughout the complex. Amphibolite, decimeters to meters thick, occurs as concordant sill-like body, and alternates with pelitic and psammitic layers. In the migmatitic gneiss, two types of quartzo-feldspathic segregations are recognized: (1) a few cm-long lenses generally conformable with the foliation and associated with mm-thick biotite-rich schlierens (Fig. 2a); and (2) irregular veins of variable thickness (1-20 mm) cross-cutting the foliation (Fig. 2b). The former lenses may represent the *in-situ* leucosomes.

The representative mineral assemblages of the Hyeondong gneiss complex are: quartz+plagioclase

+biotite± garnet± sillimanite for banded gneiss; hornblende+plagioclase+quartz+biotite+garnet +opaque phase for hornblende-biotite schist. Leucosomes of migmatitic gneiss consist of quartz +plagioclase+K-feldspar+biotite+muscovite, while melanosomes are primarily composed of biotite+sillimanite+pinitized cordierite+quartz.

The Yuli group in the study area primarily consists of alternating layers of meta-sandstone and -siltstone, or biotite-muscovite phyllite and schist. Further classification of this group is not attempted because of significant variations in lithology and thickness of constituent metasedimentary rocks. The Yuli group commonly shows the deformation fabrics such as small-scale folds and kink bands. Major metamorphic minerals include biotite, chlorite, muscovite, plagioclase and quartz. Titanite, and other opaque minerals occur as accessory phases. Micaceous pseudomorphs after cordierite and/or andalusite are common in some of metapelitic layers.

The Hongjesa granitic pluton varies from biotite granite in the central part to biotite-muscovite granite in the marginal part. Muscovite-tourmaline granite sporadically occurs in the central part, while migmatitic granite enriched in biotite locally develops at the margin of the pluton. The chloritization of biotite and the sericitization and saussuritization of plagioclase are ubiquitous. The detailed petrographic and mineral chemistries of the Hongjesa granite are described in the accompanying paper (Kim and Cho, 1994).

The xenoliths in the Hongjesa granite are rounded or ellipsoidal, and range up to 2-3 m in the maximum dimension. Most xenoliths occur near the boundary with the country rock. These xenoliths consist of meta-siltstone, surmicaceous meta-pelite and amphibolite. Petrographic and mineralogic characteristics of the xenoliths are nearly identical with those of the country rocks.

At the contact between the Yuli group and the Hongjesa granite, the surmicaceous xenolith is partially melted and consists of biotite+muscovite +sillimanite+K-feldspar+quartz+plagioclase. The absence of contact metamorphic aureole as well as the low metamorphic grade of the Yuli group suggest that the Hongjesa granite may be in fault-contact with the Yuli group.

MINERALOGY

The compositions of metamorphic minerals in various rock types of the study area were analyzed using an electron microprobe (Kim and Cho, 1994). To minimize the effect of alteration, biotites with the K content greater than 0.9 cations per formula unit (p.f.u.) on 11 anhydrous oxygen basis are only considered. Representative compositions of the analyzed minerals are given in Tables 1 to 4. The whole set of analytical data is available in Kim (19 94). For further details on the anayltical technique, refer to Lee and Cho (1992).

Plagioclase

Plagioclase in the Hongjesa granite is the albite-oligoclase solid solution. Plagioclase of biotite granite is An_{17-28}, while that of biotite-muscovite granite is An_{11-18}. Most plagioclase grains of the Hongjesa granite are altered by sericitization or saussuritization. Plagioclase in contact with K-feldspar as well as plagioclase inclusion in K-feldspar are always enriched in the albite component. The Ab-rich rim is free of sericitization or saussuritization, and may have crystallized contemporaneously with sericite. Fine grains of carbonate, mica and epidote formed by saussuritization randomly occur within plagioclase. The random orientation of micas suggests that the Hongjesa granite is little deformed during and/or after the sericitization.

The compositions of plagioclase in the Hyeondong gneiss complex range from andesine to labradorite (An_{34-60}). One cummingtonite-garnet gneiss of the Hyeondong gneiss complex has an exceptionally An-rich plagioclase (An_{92-94}). The sericitization of plagioclase is minor in the Hyeondong gneiss complex. Rare plagioclase occurs in the Yuli group.

Table 1. Representative anayses of muscovite

	Primary muscovite					Secondary muscovite replacing biotite					Secondary muscovite replacing plagioclase				
Sp. no.	1-10	4-1	5-20	721	905	227	708	709	922	923	6-2	201	227	302	709
SiO_2	45.29	46.60	45.69	46.40	45.02	49.35	45.70	45.61	46.62	46.81	45.50	45.49	47.54	45.69	45.76
Al_2O_3	35.31	35.56	35.95	35.89	35.52	29.00	34.32	30.63	33.45	29.53	37.66	37.36	36.49	35.14	36.72
TiO_2	0.54	0.92	0.07	0.52	0.35	0.02	0.37	0.23	0.79	0.15	0.00	0.00	0.00	0.52	0.00
FeO	0.91	0.83	1.71	1.10	1.40	3.52	1.84	5.02	1.40	3.21	0.03	0.90	0.53	1.05	0.18
MgO	0.26	0.78	0.25	0.31	0.46	1.31	0.73	1.82	0.91	2.23	0.00	0.27	0.01	0.65	0.03
MnO	0.03	0.01	0.00	0.03	0.01	0.04	0.00	0.08	0.03	0.05	0.00	0.02	0.00	0.02	0.07
CaO	0.02	0.02	0.01	0.01	0.00	0.09	0.01	0.04	0.03	0.04	0.00	0.03	0.04	0.00	0.00
Na_2O	0.58	0.48	0.64	0.00	0.55	0.01	0.22	0.15	0.43	0.08	0.26	0.21	0.24	0.42	0.34
K_2O	11.26	10.88	11.08	11.16	9.68	10.89	11.41	10.89	10.60	11.71	11.40	9.86	10.00	9.93	10.92
Total	94.20	96.08	95.40	95.42	92.99	94.23	94.60	94.47	94.26	93.81	94.85	94.14	94.85	93.42	94.02
Number of cations on the basis of 11 anhydrous oxygens															
Si	3.060	3.073	3.054	3.082	3.057	3.349	3.087	3.138	3.139	3.221	3.030	3.037	3.135	3.084	3.068
Al^{IV}	0.940	0.927	0.946	0.918	0.943	0.561	0.913	0.862	0.861	0.779	0.970	0.963	0.865	0.916	0.932
Subtotal	4.000	4.000	4.000	4.000	4.000	4.000	4.000	4.000	4.000	4.000	4.000	4.000	4.000	4.000	4.000
Al^{VI}	1.875	1.840	1.888	1.894	1.902	1.670	1.823	1.624	1.796	1.619	1.988	1.979	1.975	1.883	1.973
Ti	0.027	0.046	0.003	0.026	0.018	0.001	0.019	0.012	0.040	0.008	0.000	0.000	0.000	0.026	0.000
Fe	0.051	0.045	0.095	0.061	0.079	0.200	0.104	0.289	0.079	0.185	0.001	0.050	0.029	0.059	0.010
Mg	0.027	0.076	0.025	0.030	0.047	0.132	0.073	0.187	0.091	0.229	0.000	0.026	0.000	0.065	0.003
Mn	0.002	0.001	0.000	0.002	0.000	0.003	0.000	0.005	0.002	0.003	0.000	0.001	0.000	0.001	0.004
Subtotal	1.982	2.008	2.011	2.013	2.046	2.006	2.019	2.117	2.008	2.044	1.989	2.056	2.004	2.034	1.990
Ca	0.002	0.001	0.001	0.001	0.000	0.006	0.001	0.003	0.002	0.003	0.000	0.002	0.003	0.000	0.000
Na	0.075	0.061	0.083	0.000	0.072	0.001	0.029	0.021	0.056	0.011	0.034	0.028	0.031	0.055	0.044
K	0.970	0.915	0.994	0.945	0.838	0.943	0.983	0.955	0.910	1.028	0.968	0.839	0.841	0.855	0.934
Subtotal	1.047	0.977	1.028	0.946	0.910	0.950	1.013	0.979	0.968	1.042	1.002	0.869	0.875	0.910	0.978

K-feldspar

Blue-greyish K-feldspar of the Hongjesa granite is euhedral to subhedral and commonly exsolves into almost pure albite and microcline. Perthitic megacrysts have many inclusions of plagioclase, biotite, quartz and muscovite, and their size reaches up to 20 cm in some pegmatites. K-feldspar is rare in the Yuli group, while migmatitic gneiss of the Hyeondong gneiss complex contains medium to coarse porphyroblasts of K-feldspar. These K-feldspar grains are often poikiloblastic similar to those of the Hongjesa granite.

Biotite

Biotite is ubiquitous in the Hongjesa granite, and its Al content and X_{Fe} (=Fe/(Fe+Mg)) value increase from biotite granite to biotite-muscovite granite (Kim and Cho, 1994). Biotite is commonly chloritized and enriched in the Al content by alteration. The chloritization of biotite accompanies the formation of minute granules of K-feldspar, as described by many early workers (*e.g.*, Chayes, 1955; Deer *et al.*, 1965). Secondary opaque minerals such as ilmenite or pyrite develop along the cleavage plane or grain boundary of the altered biotite. In some grains of intensively-chloritized biotite, ilmenite rimmed by titanite occurs. Secondary epidote with the $Fe^{3+}/(Fe^{3+}+Al)$ ratio of 0.15-0.20 often occurs around and/or within biotite.

Biotite together with muscovite define the foliations of the Yuli group and the Hyeondong gneiss complex. The alteration of biotite in these rock units is minor in contrast to that in the Hongjesa granite.

Muscovite

Muscovite commonly occurs as both primary and secondary phases in the biotite-muscovite granite of the Hongjesa granitic pluton. Primary muscovite is nearly ideal in its composition, while secondary one is enriched in the Si and Fe+Mg contents (Table 1). Secondary muscovite replaces biotite as fine to coarse flakes, and plagioclase or K-feldspar as fine aggregates. The former is present in the migmatitic gneiss of the Hyeondong gneiss complex and the migmatitic xenolith in the Hongjesa granite. The migmatitic xenoliths have poikiloblasts of muscovite in which quartz, biotite and plagioclase are enclosed together with minor sillimanite of fibrous and prismatic forms. Such poikiloblastic muscovite may form by the hydration reaction during the emplacement of the Hongjesa granite.

Garnet

Garnet occurs in xenoliths and in three samples of the marginal Hongjesa granite. Two samples of the biotite granite contain small garnet grains (0.02 mm), while large phenocrysts of garnet (1 cm) are present in the biotite-muscovite granite. Some amphibolites and metapelites of the Hyeondong gneiss complex also contain euhedral garnet, whose maximum size is 1 cm. Garnet of the amphibolite is poikiloblastic with inclusions of quartz, biotite, ilmenite and hornblende.

Most garnet grains are almandine-rich and compositionally-zoned. The zoning patterns of garnet vary among various rock types. Garnet from a psammitic xenolith (sp. 228) has relatively homogeneous core but compositionally-zoned rim (Fig. 3a). The minor compositional fluctuations in the core of Fig. 3a may result from the re-equilibration along fractures. The homogeneous core is attributed to the high recrystallization temperature of garnet, while the increases in the X_{Fe} value and the Mn content at the rim suggest the reequilibration during cooling (Tracy, 1978). On the other hand, garnet of the hornblende-garnet-biotite gneiss (sp. 2-32) from the

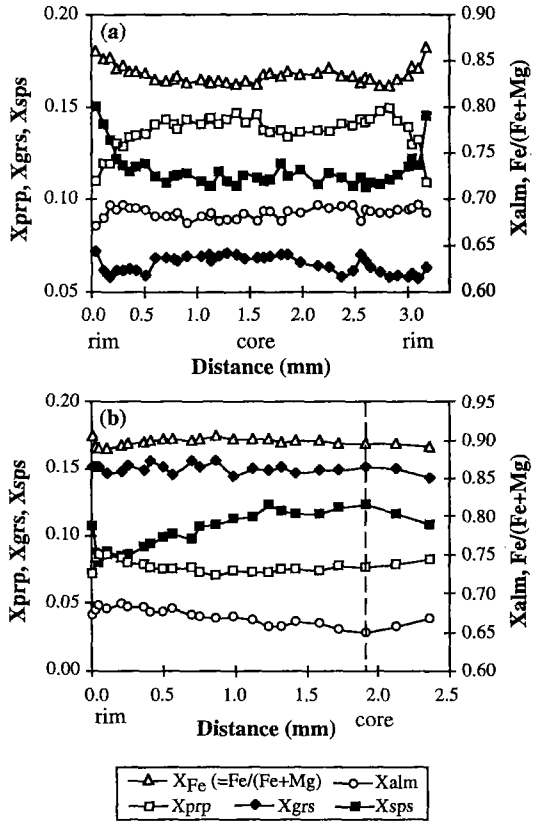

Fig. 3. Compositional zoning profiles of garnet (a) in the xenolith of the Hongjesa granite (sp. 228), and (b) in the hornblende-biotite schist of the Hyeondong gneiss complex (sp. 2-32). Symbols: open triangle, X_{Fe} (=Fe/(Fe+Mg)); open box, X_{prp} (=Mg/(Fe+Mg+Mn+Ca)); filled box, X_{sps} (=Mn/(Fe+Mg+Mn+Ca)); open circle, X_{alm} (=Fe/(Fe+Mg+Mn+Ca)); and filled diamond, X_{grs} (=Ca/(Fe+Mg+Mn+Ca)).

Hyeondong gneiss complex shows a bell-shape zoning profile where the spessartine content decreases towards the rim (Fig. 3b). The almandine content continuously increases from core to rim, while the pyrope content slightly increases towards the rim. The abrupt change in each component at the outermost rim results from the retrograde metamorphism accompanying the replacement of garnet with quartz, muscovite and chlorite.

Others

Cordierite

Cordierite occurs uncommonly in the migmatitic

gneiss of the Hyeondong gneiss complex and in one sample of the Yuli group. Most cordierite grains are altered to pinite, and positively identified by the characteristic zircon halo. Cordierite in migmatitic gneiss has inclusions of biotite, sillimanite, muscovite and quartz.

Sillimanite

The Hongjesa granite contains rare fibrolitic sillimanite surrounded by muscovite. Fibrolitic and prismatic sillimanites also occur in the xenolith and the migmatitic gneiss of the Hyeondong gneiss complex.

Amphibole

Calcic amphiboles are common in the amphibolitic rocks of the Hyeondong gneiss complex and the mafic xenoliths of the Hongjesa granite. Ferro-hornblende according to Leake (1978) predominates in the amphibolitic rocks. Ferro-actinolite occurs as alteration product in the xenolith.

DISCUSSION

Compositional variations of mica

The X_{Fe} value and the alumina content of biotite in the Hongjesa granite systematically change as the fractionation proceeds (Kim and Cho, 1994). On the other hand, significant variation in the alumina content even within single thin section is attributed to the subsolidus recrystallization. In order to decipher the mechanism affecting the Al content of biotite, several substitution mechanisms of biotite are examined (Dymek, 1983).

$(Mg, Fe)^{VI} + 2Si^{IV} \rightarrow Ti^{VI} + 2Al^{IV}$:
Ti-tschermakitic substitution (1)

$(Mg, Fe)^{VI} + Si^{IV} \rightarrow Al^{VI} + Al^{IV}$:
Tschermakitic substitution (2)

$3(Mg, Fe)^{VI} \rightarrow 2Al^{VI} + \square^{VI}$:
Dioctahedral substitution (3)

$(Mg, Fe)^{VI} + Si^{IV} \rightarrow (Fe^{3+})^{VI} + Al^{IV}$:
Ferri-tschermakitic substitution (4)

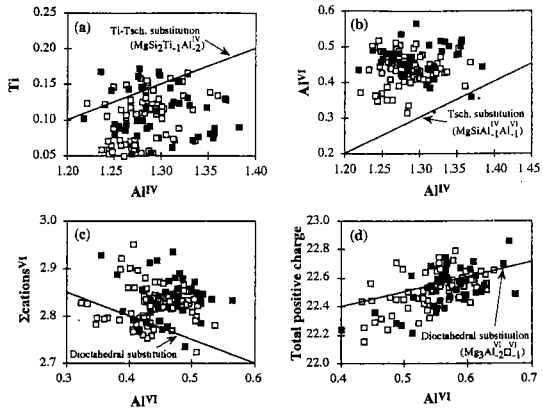

Fig. 4. Plots of biotite compositions in terms of (a) Ti-Al^{IV}; (b) Al^{IV}-Al^{VI}; (c) total octahedral cations-Al^{VI}; and (d) total positive charge-Al^{VI}. Data points of (a), (b), and (c) are calculated on the basis of 11 anhydrous oxygens, and those of (d) based on 7 cations. The reference lines represent the ideal substitutions. Symbols: open box, biotite granite; and filled box, biotite-muscovite granite.

Fig. 4 shows the compositions of biotite in terms of each substitutional scheme, and the reference line represents the ideal substitutional trend. The poor correlation between Ti and Al contents of biotite suggests that the Ti-tschermakitic substitution (1) is insignificant (Fig. 4a). Fig. 4b shows that the tschermakitic substitution (2) may be operative but insufficient to account for the Al^{VI} enrichment in biotite. This observation may be accounted for by dioctahedral substitution (3) (Fig. 4c and d). As the dioctahedral substitution involves the octahedral vacancy, it produces less than 3 total cations of octahedral coordination on the basis of 11 anhydrous oxygens. As shown in Fig. 4c, the total sum of octahedral cations generally decreases with increasing Al^{VI}. The deviation from the reference line may result from the tschermakitic substitution in biotite.

In the presence of octahedral vacancies in biotite, formula calculations based on 7 cations will overestimate the total positive charge in proportion to the number of vacancies (Dymek, 1983). This relationship is shown in Fig. 4d, where total positive charge based on 7 cations is proportional to Al^{VI}. Hence the Al^{VI} in biotite may

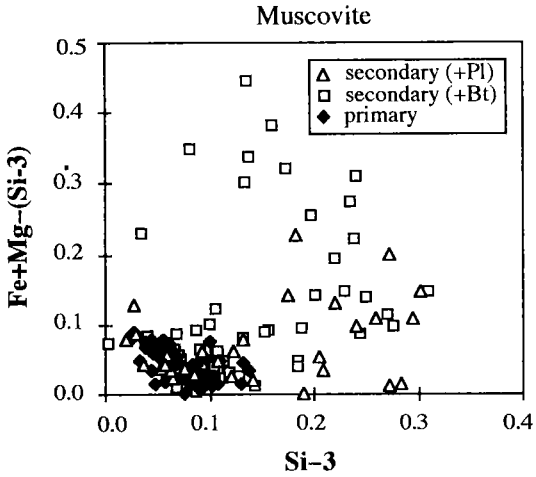

Fig. 5. Compositions of muscovite from the Hongjesa granite. Abscissa and ordinate represent the celadonitic (Si-3) and trioctahedral (Fe+Mg-(Si-3)) components, respectively.

be incorporated by the dioctahedral substitution. The total positive charge used in Fig. 4d is calculated assuming that all iron is ferrous. If the iron is partly present as ferric, the positive charge should increase. In the absence of chemical data for Fe^{3+}, it is assumed that the ferri-tschermakitic substitution (4) involving Fe^{3+} is minor.

Although some of the biotite compositions can be affected by the submicron-scale intergrowth of various sheet silicates, the compositional variation of biotite in the Hongjesa granite is primarily accounted for by the tschermakitic and dioctahedral substitutions. This observation is consistent with the petrographic evidence that biotite is often replaced by secondary muscovite, and the fact that the dioctahedral component maximizes in biotite coexisting with muscovite (Dymek, 1983).

The composition of muscovite generally deviates from the ideal one ($KAl_3Si_3O_{10}(OH)_2$) through tschermakitic (or phengitic) substitution, $Al^{VI}+Al^{IV} \rightarrow (Mg, Fe)^{VI}+Si^{IV}$, and trioctahedral substitution, $2Al^{VI}+\square^{VI} \rightarrow 3(Mg, Fe)^{VI}$ (Table 1). Fig. 5 shows the relative significance of both substitutional mechanisms. The tschermakitic substitution can be represented by the Si-3 on the basis of 11 anhydrous oxygens (Miyashiro and Shido, 1985). The trioctahedral substitution is approximated as the value of Fe+Mg-(Si-3). Primary muscovite is close to the ideal composition, but secondary one commonly deviates from the ideal composition. The enrichment in trioctahedral component may reflect the inheritance of muscovite from biotite, consistent with the textural evidence. This relationship suggests that the chemistry of retrograde mica is highly dependent on the chemistry of its parent phase (Dempster, 1992). Such compositional trend of muscovite coincides with the experimental results of Monier and Robert (1986): muscovite crystallized at high temperature is close to the ideal composition, whereas muscovite at low temperature is enriched in the phengitic component. The significant variation in the muscovite composition within a single specimen clearly demonstrates an overall lack of equilibration during the recrystallization of mica.

Geothermobarometry

Metamorphic temperature and pressure are estimated on the basis of geothermobarometry and phase relation. Five different geothermobarometers were used: garnet-biotite (Hodges and Spear, 1982); garnet-hornblende (Graham and Powell, 1984); plagioclase-muscovite (Green and Usdansky, 1986); two-feldspar (Fuhrman and Lindsley, 1988; Elkins and Grove, 1990); garnet-plagioclase-biotite-quartz(-muscovite) (Hoisch, 1990); and garnet-hornblende-plagioclase-quartz (Kohn and Spear, 1990). We use the rim composition of garnet, and the lowest X_{Fe} value at the margin of the retrograded garnet (Fig. 3b) in order to remove the retrograde effect at the outermost rim. Biotite and muscovite are relatively homogeneous, and their rim compositions are used for geothermobarometry. For plagioclase, the rim compositions are also used. The results are summarized in Fig. 6. The scattered pattern in Fig. 6 implies that the subsolidus resetting is incomplete or the estimated temperature is representative of the local equilibrium. Nevertheless, a few temperature ranges are notable in the Hongjesa granite and the Hyeondong gneiss

Table 2. Temperatures estimated from the garnet-biotite geothermometer (Hodges and Spear, 1982)

	Sp. no.	Biotite	Garnet					T (℃)
		X_{Fe}	X_{Fe}	X_{alm}	X_{prp}	X_{sps}	X_{grs}	
Hongjesa granite	302	0.611	0.918	0.733	0.065	0.163	0.039	511
		0.618	0.914	0.744	0.070	0.156	0.030	533
	(rim)	0.613	0.939	0.691	0.045	0.229	0.035	433
	958	0.777	0.936	0.789	0.054	0.141	0.015	696
	(rim)	0.781	0.954	0.803	0.039	0.136	0.022	560
Xenolith in the Hongjesa granite	228	0.487	0.820	0.686	0.151	0.127	0.036	642
		0.516	0.829	0.687	0.142	0.113	0.059	673
	(rim)	0.516	0.873	0.692	0.101	0.144	0.063	555
Hyeondong gneiss complex	2-32	0.607	0.896	0.675	0.078	0.099	0.148	632
		0.565	0.886	0.667	0.086	0.097	0.150	612
	(rim)	0.566	0.907	0.674	0.069	0.109	0.148	544
	2-42	0.643	0.899	0.763	0.086	0.080	0.071	646
		0.666	0.893	0.753	0.090	0.063	0.094	718
		0.649	0.893	0.750	0.090	0.074	0.086	692
	2-45	0.568	0.898	0.670	0.076	0.086	0.168	583
		0.566	0.886	0.656	0.084	0.089	0.171	622
		0.575	0.927	0.619	0.049	0.177	0.155	486
	3-24	0.465	0.789	0.734	0.196	0.004	0.066	704
		0.480	0.812	0.757	0.175	0.006	0.062	668

complex.

The temperature of the Hyeondong gneiss complex is calculated at an assumed pressure of 4 kbar (see below for further details on the pressure estimate), using the garnet-biotite geothermometry. Compositions of garnet and biotite together with the estimated temperatures are presented in Table 2. The variation in pressure hardly affects the temperature estimate that changes in the order of 10℃ over the 2 kbar range. Because the modal amount of biotite is far greater than that of garnet, the compositions of biotite should be less affected by reequilibration than those of garnet. Thus the temperature calculated from the core composition of garnet may represent the peak metamorphic condition.

The temperature of the Hyeondong gneiss complex ranges from 593℃ to 718℃ using the garnet-biotite geothermometer (Fig. 6a). The retrograde temperature using the outermost rim composition of garnet vary from 486℃ to 562℃. The compositions of garnet core and matrix biotite from a banded gneiss (sp. 2-42) yield temperatures of 681-718℃. This high temperature range is consistent with the occurrence of high-grade mineral assemblage, cordierite+sillimanite+biotite +K-feldspar+plagioclase+quartz, in the Hyeondong gneiss complex. Temperatures estimated from the garnet-hornblende geothermometer are lower than those from the garnet-biotite geothermometer (Table 3). This apparent discrepancy may result from either slow diffusion rate of Ca in garnet (p. 612, Spear, 1993) or the effect of other components in amphibole solid solution.

The garnet porphyroblast in the psammitic xenolith of the Hongjesa granite lacks chemical zoning because of homogenization during the emplacement of the Hongjesa granite (Fig. 3a; Yardley, 1977; Spear, 1989). Temperatures estimated from the xenolith range from 524℃ to 673℃ (Fig. 6b). Matrix biotite together with the core compositions of garnet yield the maximum

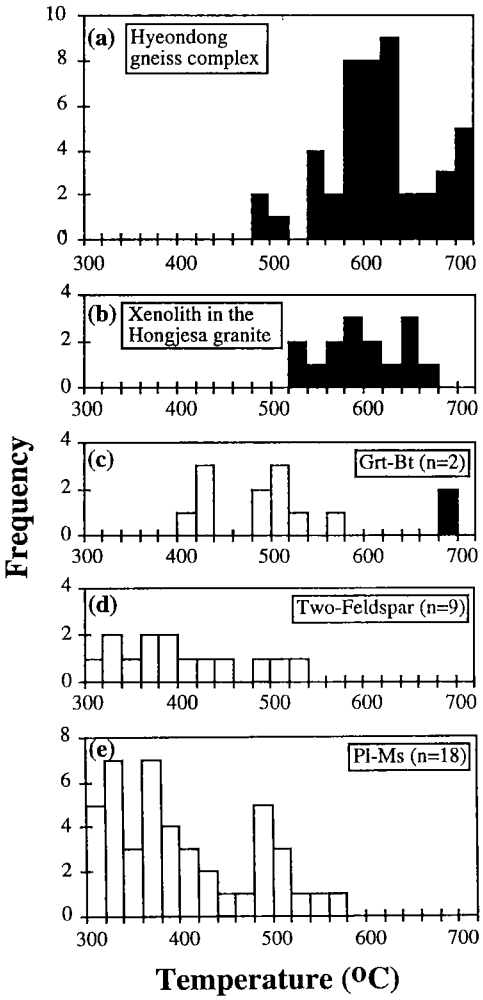

Fig. 6. Frequency diagrams showing the result of geothermometric calculations in the Hyeondong gneiss complex (a), the xenolith in the Hongjesa granite (b), and the Hongjesa granite itself (c-e). The closed boxes represent temperatures from the garnet-biotite geothermometry and open boxes denote recrystallization temperatures of the Hongjesa granite using garnet-biotite (c), two-feldspar (d), and plagioclase-muscovite (e) geothermometers. 'n' represents the number of the samples analyzed for each geothermometry.

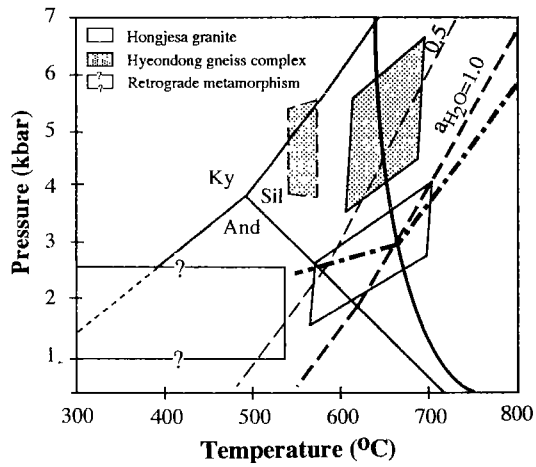

Fig. 7. Petrogenetic grid showing the P-T ranges estimated for the Hongjesa granite and the Hyeondong gneiss complex. Shaded box represents the P-T conditions of the Hyeondong gneiss complex estimated from the garnet-biotite-plagioclase-quartz geobarometer and garnet-biotite geothermometer, while that with dashed outline from garnet-hornblende-plagioclase-quartz barometer and garnet-hornblende thermometer. Open boxes designate the P-T conditions for the emplacement and the subsolidus recrystallization of the Hongjesa granite, respectively. Heavy curve is the melting curve of haplogranite after Ebadi and Johannes (1991). Dashed curve is the muscovite-breakdown reaction calculated from the TWEEQU program (Berman, 1991) using the muscovite composition of this study. Dot-dashed curve represents the cordierite-forming reaction (biotite + sillimanite = cordierite + K-feldspar + H_2O) adopted from Vielzeuf and Holloway (1988). Aluminum silicate triple point is from Holdaway (1971).

temperature of 673℃ in sp. 228 (Table 2). Retrograde metamorphic temperatures using the outermost rim composition of garnet together with matrix biotite range from 524℃ to 583℃. The garnet-hornblende temperature estimated from the amphibolitic xenolith (sp. 218; Table 3) ranges from 477℃ to 530℃.

Temperatures of the Hongjesa granite are estimated using garnet-biotite, two-feldspar, and plagioclase-muscovite geothermometers (Fig. 6c-e). The garnet-biotite geothermometry in two garnet-bearing biotite granites (Fig. 6c) yields variable temperatures ranging from 408℃ to 696℃ at an assumed pressure of 3 kbar (see below). The high temperature estimates of 682℃ and 696℃ are similar to those from the xenolith and may correspond to the emplacement temperature of the Hongjesa granitic magma.

Temperatures estimated from two-feldspar and plagioclase-muscovite geothermometries range from 310℃ to 568℃ (Fig. 6d and e). Because of

Table 3. Temperatures estimated from the garnet-hornblende geothermometer (Graham and Powell, 1984)

	Sp. no.	Garnet		Hornblende	lnK_d	T (℃)
		X_{Fe}	X_{grs}	X_{Fe}		
Hyeondong gneiss complex	2-32	0.920	0.144	0.607	2.01	483
		0.915	0.142	0.632	1.84	512
		0.899	0.143	0.591	1.82	516
	2-45	0.890	0.176	0.597	1.70	565
		0.890	0.163	0.597	1.70	555
		0.886	0.171	0.597	1.66	569
Xenolith in the Hongjesa granite	218	0.946	0.268	0.648	2.25	530
		0.946	0.269	0.567	2.59	477
		0.947	0.268	0.632	2.34	515

Table 4. Pressures estimated from the garnet-plagioclase-biotite-quartz geobarometer (Hoisch, 1990) and the garnet-hornblende-plagioclase-quartz (Kohn and Spear, 1990) using the GIBBS program (Spear and Menard, 1989)

	Sp. no.	Garnet				Plagioclase	Biotite	Hornblende		T (℃)	P (kbar)
		X_{alm}	X_{prp}	X_{grs}	X_{sps}	X_{an}	X_{Fe}	Si*	X_{Fe}		
Hyeondong gneiss complex	2-42	0.761	0.093	0.070	0.076	0.450	0.646			605	3.6
		0.778	0.077	0.057	0.087	0.396	0.650			698	6.6
	3-24	0.775	0.156	0.063	0.006	0.944	0.480			610	3.7
		0.757	0.175	0.062	0.006	0.928	0.465			664	4.5
	2-45	0.661	0.082	0.176	0.081	0.476		6.714	0.581	565	4.9
		0.656	0.084	0.171	0.089	0.499		6.715	0.579	569	4.6
Hongjesa granite	958	0.803	0.039	0.022	0.136	0.135	0.781			560	2.8
		0.789	0.055	0.015	0.141	0.147	0.777			690	2.9

*Si calculated on the basis of 23 cations.

the subsolidus compositional resetting, these geothermometers yield low temperatures. The broad range in the estimated temperatures together with textural evidence suggest that secondary minerals are not fully equilibrated during retrograde metamorphism.

Pressures were estimated using garnet-hornblende-plagioclase-quartz (Kohn and Spear, 1990) and garnet-plagioclase-biotite-quartz (-muscovite) (Hoisch, 1990) geobarometers. The results are summarized in Table 4 and shown in Fig. 7. Both geobarometers yield the pressure of 3.6-6.6 kbar for the Hyeondong gneiss complex. The lack of mineral assemblages suitable for geothermobarometry hardly allows us to estimate the metamorphic condition of the Yuli group.

In summary, the peak metamorphic condition of the Hyeondong gneiss complex is 593-718℃ and 3.6-6.6 kbar, which correspond to the upper amphibolite facies. Following the emplacement, the Hongjesa granite has been affected by the subsolidus reequilibration at 310-568℃.

Hong (1992) has estimated the emplacement pressure of the Hongjesa granite to be 1-3 kbar, using the quartz-orthoclase-albite-H_2O system. However, this pressure estimate is subject to large uncertainties because of the unknown effect of other components such as F, B and CO_2 (Manning and Pichavant, 1988). Pressures calculated from the garnet-plagioclase-biotite-quartz geobarometer in the garnet-bearing biotite granite range from 1.5-4.0 kbar (Fig. 7; Table 4). The significant

variation in the pressure estimate is attributed to the partial reequilibration of the geobarometric assemblage during the retrograde stage. In order to better estimate the pressure of the Hongjesa granite, metamorphic phase equilibria of xenoliths are used together with the geobarometric calculation. In the migmatitic xenolith, muscovite poikiloblasts enclosing sillimanite represents the hydration reaction:

$$\text{sillimanite} + \text{K-feldspar} + H_2O = \text{muscovite} + \text{quartz} \quad (5)$$

The location of the reaction (5) in Fig. 7 is calculated from the TWEEQU program (Berman, 1991), using the analyzed composition of muscovite. The intersection point between this reaction curve and the granitic solidus curve (Ebadi and Johannes, 1991) defines the minimum pressure of the Hongjesa granite to be about 3 kbar, because both reaction curves are dependent on the activity of H_2O (a_{H_2O}). The consistency of this minimum pressure with the geobarometric result as well as the common occurrence of pegmatitie veins or dykes suggest that a_{H_2O} of the Hongjesa granitic magma is close to unity during the granite emplacement. Therefore, we conclude that the Hongjesa granite has been emplaced at 650-700℃ and 3±1 kbar under the H_2O-saturated condition.

Garnet zoning profile and P-T path

In order to decipher the P-T change during the garnet growth, some garnet grains in several xenoliths and metasedimentary rocks were analyzed in detail. In contrast to others, garnet porphyroblasts of the Hyeondong gneiss complex show complex zoning patterns. The zoning profile of garnet in sp. 2-42 indicates two-stage growth history (Fig. 8). The inner part of garnet has no apparent chemical zoning because of the fast diffusion rate at temperatures above 650℃ (Yardley, 1977; Spear, 1991). In the outer part, however, garnet is significantly zoned. In particular, the abrupt change in the grossular content is notable at the margin. The Ca content

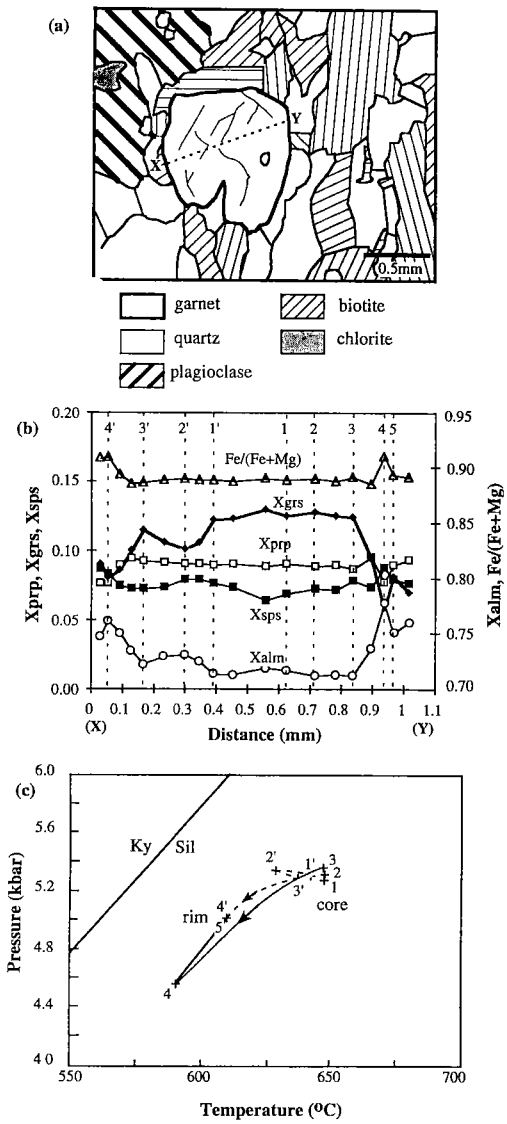

Fig. 8. (a) A sketch of the garnet-bearing assemblage in sp. 2-42. Dotted line (X-Y) represents the analyzed section; (b) Compositional variation of garnet along the X-Y section of (a). Symbols are the same as in Fig. 3. The numbers at the top refers to the analytic positions used for the Gibbs' calculation; (c) P-T path calculated from the garnet compositions shown in (b), using the Gibbs' method. Dashed and solid curves represent the P-T paths calculated from the left and right halves of the zoning profile in (b), respectively. The arrows denote the P-T changes from core to rim of garnet.

of plagioclase sympathetically varies with that of garnet (Table 5). Such chemical zonings in garnet

Table 5. Compositions of garnet and plagioclase in sp. 2-42 used for the Gibbs' calculation

Analytic point no. of garnet*	X_{alm}	X_{grs}	X_{an}**
1	0.718	0.129	0.394
2	0.712	0.128	0.404
3	0.712	0.123	0.396
4	0.778	0.057	0.425
5	0.750	0.081	0.448
1′	0.713	0.123	0.394
2′	0.730	0.101	0.404
3′	0.772	0.114	0.396
4′	0.761	0.080	0.425

*See Fig. 8 for the analytic point of garnet. **The X_{an} values represent the compositions of plagioclase, which are assumed to be in equilibrium with the composition corresponding to each analytic point of garnet.

and plagioclase indicate that the Hyeondong gneiss complex may have experienced poly-metamorhism as suggested by Kim *et al.* (1986).

It is critical to understand the reaction history of the sample before interpreting the origin of chemical zoning in a mineral (Frost and Tracy, 1991; Spear, 1993). However, the absence of any inclusion except quartz in garnet and the high-variance nature of sp. 2-42 do not allow us to determine the reaction governing the formation and compositional zoning of garnet. Nevertheless, qualitative P-T history may be inferred from the zoning profiles of garnet and plagioclase using the Gibbs' method (Spear and Selverstone, 1983). We performed the thermodynamic calculation using the GIBBS program (Spear and Menard, 1989). The high-variance assemblage garnet+plagioclase +biotite+quartz for sp. 2-42 suggests that the growth of garnet may be modelled by the net-transfer reaction, pyrope + 2 grossular + eastonite + 2 quartz = 2 anorthite + phlogopite (Hoisch, 1990), and the $FeMg_{-1}$ exchange reaction between garnet and biotite. In the system Al_2O_3-SiO_2-FeO-MgO-CaO-H_2O, the variance of the assemblage garnet+biotite+plagioclase+quartz+H_2O is three. The variables chosen are X_{alm} (=Fe/(Fe+Mg+Mn+Ca)) and X_{grs} (=Ca/(Fe+Mg+Mn+Ca)) of garnet, and the An content of plagioclase. Initial P-T condition of 610℃ and 5 kbar is estimated from the geothermobarometry using the compositions of garnet rim and matrix biotite. Changes in two independent parameters (X_{alm} and X_{grs}) are available from the chemical zoning of garnet. Changes in the third parameter, X_{an} (=Ca/(Ca+Na)), are inferred by examining of the zoning profile of plagioclase. The compositions of garnet and plagioclase used for the calculation are listed in Table 5.

The result is shown in Fig. 8c. Although the P-T variation is minor and the P-T paths from the left and right halves of Fig. 8b are not identical, the core-to-rim path suggests that garnet may have experienced a complex growth history. The discrepancy in the calculated P-T paths results from the asymmetric zoning profile of garnet, particularly in the grossular content, and the difficulty in determining the equilibrium compositions between garnet and plagioclase. Because of the uncertainties involved in our simple calculation, the P-T path obtained from the Gibbs' method is only qualitative.

Migmatization of the Hyeondong gneiss complex

The Hyeondong gneiss complex is locally migmatitic. The term 'migmatite' here is descriptive, and represents the rock in which melanosome and leucosome are distinguishable (Ashworth, 1985). The degree of migmatization in the Hyeondong gneiss complex is variable on the order of a few meters (Fig. 2).

In order to understand the origin of migmatite, it is necessary to determine whether leucosomes are formed by metamorphic differentiation or external magmatic melt or internal anatectic melt. The presence of anatectic melt can be identified using petrographic and textural criteria of Mclellan (1989). The leucosomes in migmatitic gneiss of the Hyeondong gneiss complex show no internal deformational fabric. Quartz is free of recrystallization, and synneusis of plagioclase is commonly observed. Small aspect ratio of individual minerals in leucosome suggests the growth in the presence of melt (Mclellan, 1988, 1989). Minor

partial melting is apparent in leucocratic domains, as evidenced by anhedral quartz and cloudy perthitic K-feldspar (Pattison and Harte, 1988). The subspherical leucosomes enclosed by melanosomes argue against the injection of externally-derived melt. The vein-like leucosomes are also observed. These petrographic observations indicate that the leucosome has crystallized from an *in-situ* melt formed by partial melting of metapelite.

The leucosome is composed of quartz, K-feldspar, plagioclase and minor biotite. Perthitic K-feldspar is poikiloblastic, and includes anhedral quartz and plagioclase with albite-rich rim. Melanosome consists primarily of biotite, sillimanite and cordierite together with minor amounts of quartz, plagioclase, zircon, apatite and tourmaline. Cordierite coexisting with biotite and sillimanite in melanosome defines the reaction:

$$\text{biotite} + \text{sillimanite} + \text{quartz} = \text{cordierite} + \text{K-feldspar} + H_2O \quad (6)$$

(Holdaway and Lee, 1977; Vielzeuf and Holloway, 1988), and its P-T location is given in Fig. 7. K-feldspar formed by the reaction (6) may form poikiloblast in leucosome. Because this reaction depends on a_{H_2O} in both fluid and cordierite, it provides only qualitative P range of 2.5-4 kbar at temperatures of 593-718℃ estimated for the Hyeondong gneiss complex. However, the reaction (6) does not proceed significantly because biotite is common in migmatitic gneiss. The absence of garnet in the migmatitic gneiss of the Hyeondong gneiss complex corroborates the relatively low pressure condition during the migmatization (Le Breton and Thompson, 1988; Vielzeuf and Holloway, 1988).

CONCLUSIONS

The Hongjesa granite has been emplaced at 650-700℃ and 3± 1 kbar, and experienced the subsolidus recrystallization at 310-568℃. During the subsolidus stage, biotite changes its Al content through tschermakitic and dioctahedral substitution. Secondary muscovite is enriched in the Si and Mg+Fe contents by tschermakitic and trioctahedral substitutions.

The Hyeondong gneiss complex has experienced the upper amphibolite facies metamorphism at 593-718℃ and 3.6-6.6 kbar. The local migmatization in the Hyeondong gneiss complex results from the partial melting probably accompanying the cordierite-forming reaction. The heterogeneous compositional zoning of garnet and plagioclase together with the P-T path using the Gibbs' method suggest that the Hyeondong gneiss complex may have experienced poly-metamorphism.

ACKNOWLEDGMENTS

This paper constitutes one chapter of an M.Sc. thesis of the first author at Seoul National University and was supported by the Basic Science Research Institute Program, Ministry of Education, 1993, Project No. BSRI-93-504. We thank Kyoungwon Min and Myeonghyo Kang for their field assistance, and Chang Whan Oh and Bognam Ree for their constructive reviews.

REFERENCES

Ashworth, J.R., 1985, Migmatites. Blackie, New York, 302p.

Berman, R.G., 1991, Thermobarometry using multi-equilibrium calculations: a new technique with petrological applications. Canadian Mineral., 29, 833-855.

Chayes, F., 1955, Potash feldspar as a by-product of the biotite-chlorite transformation. Jour. Geol., 63, 75.

Deer, W.A., Howie, R.A. and Zussman, J., 1965, Rock forming minerals. Vol. 3, Sheet silicates, Longman, London, 266p.

Dempster, R.F., 1992, Zoning and recrystallization of phengitic micas: Implications for metamorphic equilibration. Contrib. Mineral. Petrol., 109, 526-537.

Dymek, R.F, 1983, Titanium, aluminum and interlayer cation substitutions in biotite from high grade gneisses, west Greenland. Am. Mineral., 68, 880-899.

Ebadi, A. and Johannes, W., 1991, Beginning of melting and composition of first melts in the system Qz-Ab-Or-H_2O-CO_2. Contrib. Mineral. Petrol., 106, 286-295.

Elkins, L.T. and Grove, T.L., 1990, Ternary feldspar experiments and thermodynamic models. Am. Mineral., 75, 544-559.

Frost, B.R. and Tracy, R.J., 1991, P-T paths from zoned garnets: some minimum criteria. Am. Jour. Sci., 291, 917-939.

Fuhrman, M.L. and Lindsley, S.I., 1988, Ternary feldspar modelling and thermometry. Am. Mineral., 73, 201-215.

Graham, C.M. and Powell, R., 1984, A garnet-hornblende geothermometer: Calibration, testing, and application to the Pelona Schist, southern California. Jour. Metamorphic Geol., 2, 13-21.

Green, N.L. and Usdansky, S.I., 1986, Toward a practical plagioclase-muscovite thermometer. Am. Mineral., 71, 1109-1117.

Hodges, K.V. and Spear, F.S., 1982, Geothermometry, geobarometry and the Al_2SiO_5 triple point at Mt. Moosilauke, New Hampshire. Am. Mineral., 67, 1118-1134.

Hoisch, T.D., 1990, Empirical calibrations of six geobarometers for the mineral assemblages: Quartz + muscovite + biotite + plagioclase + garnet. Contrib. Mineral. Petrol., 104, 225-234.

Holdaway, M.J., 1971, Stability of andalusite and the aluminum silicate phase diagrams. Am. Jour. Sci., 271, 97-131.

Holdaway, M.J. and Lee, S.M., 1977, Fe-Mg cordierite stability in high grade pelitic rocks based on experimental, theoretical and natural observations. Contrib. Mineral. Petrol., 63, 175-198.

Hong, Y.K., 1992, Petrogenesis and evolution of early Proterozoic granitic rocks in the Northeastern Ryeongnam Massif, Korea. Jour. Geol. Soc. Korea, 28, 571-589.

Kim, H.S., Lee, S.M. and Lee, B.N., 1986, Petrogenesis of the Hongjesa granitic gneiss in the eastern part of Mt. Taebaeg area, Korea. Memoirs for Prof. Sang Man Lee's Sixtieth Birthday. University Text Publisher Co., Seoul, 107-133.

Kim, H.S., Lee, S.M., Kim, Y.K., Park, C.S., Kim, S.J. and Chang, H.W., 1991, Proterozoic magmatism and metamorphism in the northeastern part of Korea-Comparative studies between Buncheon and Pyeonghae granitic gneisses. Jour. Geol. Soc. Korea, 27, 614-625.

Kim, J., 1994, Petrogenetic study of the Hongjesa granite and the metasedimentary rocks in the northeastern Sobaeksan Massif. M.Sc. dissertation, Seoul National Univ.

Kim, J. and Cho, M., 1994, Petrogenesis of the Precambrain Hongjesa granite (Magmatism and metamorphism of the Proterozoic in the northeastern part of Korea). Jour. Petrol. Soc. Korea (this issue).

Kim, T.K., 1991, Petrological and geochemical studies on the Buncheon granitic gneiss and its adjacent metasedimentary rocks in the northeastern part of the Sobaeksan Massif. Ph.D. dissertation, Seoul National Univ., 128p.

Kim, Y.J. and Lee, D.S., 1983, Geochronology and petrogenesis processes of the so-called Hongjesa granite in the Seokpo-Deogku area. Jour. Korean Inst. Mining Geol., 16, 163-221.

Kohn, M.J. and Spear, F.S., 1990, Two new geobarometers for garnet amphibolites, with applications to southeastern Vermont. Am. Mineral., 75, 89-96.

Leake, B.E., 1978, Nomenclature of amphiboles. Canadian Mineral., 16, 501-520.

Le Breton, N. and Thompson, A.B., 1988, Fluid-absent (dehydration) melting of biotite in metapelites in the early stages of crustal anatexis. Contrib. Mineral. Petrol., 99, 226-237.

Lee, K.J. and Cho, M., 1992, Metamorphism of the Gyeonggi Massif in the Gapyeong-Cheongpyeong area. Jour. Petrol. Soc. Korea, 1, 1-25.

Lee, S.M. and Kim, H.S., 1984, Metamorphic studies on the so-called Yulri and Weonnam groups in the Mt. Taebaeg area. Jour. Geol. Soc. Korea, 20, 195-214.

Manning, D.A.C. and Pichavant, M., 1988, Volatiles and their bearing on the behavior of metals in granitic systems. In Recent advances in the geology of granite related mineral deposits (eds. R.P. Taylor and B.F. Strong), Canadian Inst. Mining Metal., 39, 13-24.

Mclellan, E.L., 1988, Migmatite structures in the Central Gneiss Complex, Boca de Quadra, Alaska. Jour. Metamorphic Geol., 6, 517-542.

Mclellan, E.L., 1989, Sequential formation of subsolidus and anatectic migmatites in response to thermal evolution, Eastern Scotland. Jour. Geol., 97, 165-182.

Miyashiro, A. and Shido, F., 1985, Tschermak substitution in low- and middle-grade pelitic schists. Jour. Petrol., 26, 449-487.

Monier, G. and Robert, J.L., 1986, Muscovite solid solutions in the system K_2O-MgO-FeO-Al_2O_3-SiO_2-H_2O: an experimental study at 2 kbar P_{H_2O} and comparison with natural Li-free white micas. Mineral. Mag., 50, 257-266.

Pattison, D.R.M. and Harte, B., 1988, Evolution of structurally contrasting anatectic migmatites in the 3-kbar Ballachulish aureole, Scotland. Jour. Metamorphic Geol., 6, 475-494.

Spear, F.S., 1989, Petrologic determination of metamorphic pressure-temperature-time paths. In Metamorphic pressure-temperature-time paths (eds. F.S. Spear and S.M. Peacock), Short Courses in Geology, Vol. 7, Am. Geophys. Union, 1-55.

Spear, F.S., 1991, On the interpretation of peak metamorphic temperatures in light of garnet diffusion during cooling. Jour. Metamorphic Geol., 9, 379-388.

Spear, F.S., 1993, Metamorphic phase equilibria and pressure-temperature-time paths. Monograph series, 1, Mineral. Soc. Am., 789p.

Spear, F.S. and Menard, T., 1989, Program GIBBS: a generalized Gibbs method algorithm. Am. Mineral., 74, 942-943.

Spear, F.S. and Selverstone, J., 1983, Quantitative P-T paths from zoned minerals: theory and tectonic applications. Contrib. Mineral. Petrol., 83, 348-357.

Tracy, R.J., 1978, High grade metamorphic reactions and partial melting in pelitic schist, western-central Massachusetts. Am. Jour. Sci., 278, 150-178.

Vielzeuf, D. and Holloway, J.R., 1988, Experimental determination of the fluid-absent melting relations in the pelitic system. Consequences for crustal differentiation. Contrib. Mineral. Petrol., 98, 157-276.

Yardley, B.W.D., 1977, An empirical study of diffusion in garnet. Am. Mineral., 62, 793-800.

(책임편집 : 권성택)

홍제사 화강암과 주변 변성퇴적암류의 변성작용
(한국 북동부지역의 원생대의 화성활동과 변성작용)

김정민 · 조문섭 · 김형식*

서울대학교 자연과학대학 지질과학과
*고려대학교 이과대학 지질학과

요 약 : 소백산육괴 북동부지역의 변성 진화과정을 밝히는 작업의 일환으로, 선캠브리아 홍제사 화강암 및 율리층군과 현동 편마암복합체를 연구하였다. 홍제사 화강암은 650-700℃ 와 3±1 kbar에서 관입하였으며, 310-568℃ 에서 변질작용을 받았다. 변질과정 중에 흑운모의 녹니석화 작용 뿐만 아니라 사장석의 견운모화 및 소수라이트화 작용이 일어났다. 홍제사 화강암 내의 흑운모는 마그마 고결 이후 이팔면체(dioctahedral) 치환과 처마카이트(tschermakite) 치환에 의해 Al, Fe와 Mg 양이 변한다. 이차 백운모는 처마카이트 치환과 삼팔면체(trioctahedral) 치환에 의해 Si와 (Mg+Fe) 양이 증가한다. 현동 편마암 복합체의 변성 압력, 온도조건은 593-718℃, 3.6-6.6 kbar이다. 근청석을 포함하는 광물조합을 형성시킨 혼성암화 작용이 현동 편마암복합체 내에서 국부적으로 관찰된다. 호상편마암 내의 흑운모+석류석+사장석+석영의 광물 조합에 대해 깁스(Gibbs) 방법을 적용하였을 때, 현동 편마암복합체가 복잡한 온도-압력 진화과정을 겪었음을 알 수 있다.

핵심어 : 홍제사 화강암, 현동 편마암복합체, 깁스방법, 혼성암화작용